Applied Catalysis B: Environmental 138–139 (2013) 353–361

Contents lists available at SciVerse ScienceDirect

Applied Catalysis B: Environmental

journal homepage: www.elsevier.com/locate/apcatb

Unravelling the structure and reactivity of supported Ni particles in Ni-$CeZrO_2$ catalysts

S. Gopalakrishnan[a,b], M.G. Faga[b], I. Miletto[a], S. Coluccia[a,b], G. Caputo[c], S. Sau[c], A. Giaconia[c], G. Berlier[a,*]

[a] Università di Torino, Dipartimento di Chimica and NIS Centre of Excellence, Via P. Giuria 7, Torino, 10125 Italy
[b] CNR-IMAMOTER, Strada delle Cacce 73, Torino, 10135, Italy
[c] ENEA, "Casaccia" Research Center, via Anguillarese, 301, 00123 Rome, Italy

ARTICLE INFO

Article history:
Received 31 October 2012
Received in revised form 11 February 2013
Accepted 18 February 2013
Available online 4 March 2013

Keywords:
Methane steam reforming
$CeZrO_2$
Ni carbonyls
FTIR spectroscopy
Solar energy

ABSTRACT

We report about the synthesis and characterisation of two $NiCeZrO_2$ catalysts prepared by one pot-co-precipitation method. The two samples are characterised by similar chemical composition (15 wt% Ni, Ce/Zr = 80/20 atomic ratio) and properties of the $CeZrO_2$ support, which is a cubic phase solid solution with nanometer sized (5–6 nm) crystalline hexagonal/roundish particles. The main differences between the samples are in the NiO particles dispersion and surface area, which were found to be affected by the synthesis pH. Both samples were characterised about their surface properties by employing FTIR spectroscopy of adsorbed CO probe, and tested about their activity and stability in methane steam reforming (MSR) reaction at relatively low temperature (793 K). The results show a good activity in MSR irrespective of the NiO size and morphology, with negligible CO formation, but a strong dependence of the catalysts stability upon these parameters. Only the catalyst with smaller (5–10 nm) NiO particles was found stable for 250 h in MSR at relatively high steam to carbon ratio (S/C = 2). This performance could be related to a positive effect of the $CeZrO_2$ support, allowing fast and easy oxygen transfer to and from the NiO/Ni^0 active phase, most likely thanks to the occurrence of a strong metal–support interaction.

1. Introduction

The growing request for the development and diffusion of technologies based on renewable energy sources represents an important challenge for researchers working in catalysis. In recent years, steam reforming of methane (MSR) has received a wide attention for the production of hydrogen and syngas as a major feedstock for fuel cells and Fischer-Tropsch reaction. When the process is coupled to water gas shift reaction, hydromethane (a mixture of hydrogen and methane) can be obtained, which, after CO_2 removal, could be employed to power hybrid automotive systems. If the temperature of the process is lowered by employing a proper catalyst, a low green-house impact fuel can be produced in solar powered plants, based on molten salt technology [1,2].

Commercial catalysts for the methane steam reforming reaction are based on metal Ni particles dispersed on supports such as Al_2O_3, MgO and $MgAl_2O_4$ or their mixture [3]. Selection of support material is an important issue, as it has been evidenced that it can seriously influence metal activity and stability [3–5]. This effect, mainly based on the support surface properties and metal–support interaction, can also result in low temperature activity of the Ni phases [6].

The primary difficulty associated with Ni is deactivation due to either coke formation or sintering of metallic and support phases at high temperature [7,8]. Sintering, often caused by the severe conditions of the industrial process (high temperature and pressure, necessary to shift the thermodynamic equilibrium to the products), results in the formation of large metal particles, with consequent loss in surface area ad activity. The second, but not less important cause of deactivation is related to the formation of carbon whiskers, which grow on and strongly bind to Ni particles, causing their removal from the support or even reactor blockage. This phenomenon could be reduced by increasing the steam to carbon ratio (S/C), but this would require major limitations in the process parameters and lower energy-efficiency of the plant [3]. Promoters are often employed to avoid the deactivation issue. These include alkali metal ions, sulphurs, transition metal ions (Ag, Au, Cu, Sn, etc.) or even doping with boron [9–12].

One of the most promising catalysts for low temperature MSR is based on Ni-$CeZrO_2$ mixed oxide [13–16]. CeO_2 is an active support, widely employed in catalysis thanks to the reported enhancement of metal dispersion and strong metal–support interaction (SMSI) [14,17–20]. Moreover, CeO_2 has a high "oxygen storage capability" (OSC), related to the presence of oxygen vacancies in defective

* Corresponding author. Tel.: +39 0116707856; fax: +39 0116707953.
E-mail address: gloria.berlier@unito.it (G. Berlier).

0926-3373/$ – see front matter © 2013 Elsevier B.V. All rights reserved.
http://dx.doi.org/10.1016/j.apcatb.2013.02.036

sites that can be quickly formed and destroyed [21–23]. This feature could be useful to avoid deactivation as a consequence of coke formation. At high reaction temperature, however CeO_2 is readily sintered, which results in catalyst deactivation. It has been reported that the addition of ZrO_2 leads to improvement in thermal resistance and OCS of CeO_2 [24–28]. This was found to be due to the partial substitution of Ce^{4+} with Zr^{4+} in the lattice of CeO_2, which results in a solid solution formation [29–31].

In this study, the structural and surface properties of two $NiCeZrO_2$ catalysts, prepared by optimisation of a co-precipitation method [13], are compared. The two samples are characterised by similar chemical composition (15 wt% Ni, Ce/Zr = 80/20 atomic ratio), $CeZrO_2$ crystalline structure, particle size and morphology. However, pH modification in the synthesis resulted in different specific surface area and NiO particle size. This allowed us to compare the two catalysts surface properties and reactivity, by employing FTIR spectroscopy of CO probe molecule and by performing catalytic tests in low temperature methane steam reforming. The whole set of results suggest an important effect of the $CeZrO_2$ support on the redox behaviour of NiO/Ni^0 particles, suggesting easy oxygen transfer to/from the support when in intimate contact with the active phase.

2. Experimental

2.1. Catalyst preparation

Ni-Ce-ZrO_2 catalysts were prepared through the optimisation of a one step co-precipitation/digestion method reported in the literature [13]. Ni loading was fixed at 15 wt%, while the support composition was chosen as 80 mol% of CeO_2 and 20 mol% of ZrO_2. Stoichiometric quantities of zirconyl nitrate solution (99.9%, Sigma–Aldrich), cerious nitrate (99.9% Aldrich), and nickel nitrate (99.99%, Aldrich), were dissolved in distilled water, and the resulting solution was transferred to a round-bottomed glass flask. An aqueous 20% KOH (w/w) solution was added drop-wise at 353 K with constant stirring to attain an alkaline pH, which was maintained during the entire course of co-precipitation reaction. Catalyst A was prepared at pH 10.5, while pH 9.5 resulted in catalyst B. The precipitates were digested at 353 K for 24 h. Afterwards, they were thoroughly washed with distilled water to remove potassium impurities, dried at ambient conditions for 48 h and at 393 K for 6 h. The dried mass thus obtained was then finely ground to an average particle size of less than a micron. This material was calcined at 773 K for 6 h to obtain the final catalysts.

2.2. Characterisation techniques

Specific Surface Area (SSA) was measured by nitrogen adsorption and desorption cycles at 77 K using a Micromeritics (ASAP 2020) surface area measurement apparatus, employing the Brunauer Emmet Teller model. XRD patterns were recorded using a X'Pert PRO MPD from PANalytical PW3040/60 diffractometer (Ni filtered Cu-Kα radiation, 40 kV, 35 mA) in the range of 20–80° with an angular step of 0.0167°/min at 100 s per step, using 0.3 mm capillaries. The average crystallite size of the samples was determined with the Scherrer equation from the line-widths of the XRD peaks at ca. $2\theta = 29°$, corresponding to (1 1 1) plane of cubic $CeZrO_2$, and at ca 43°, corresponding to the (2 2 0) plane of cubic NiO.

The chemical composition of the calcined samples was determined by EDX microanalysis (Oxford INCA Energy 200, connected to Zeiss EVO50 SEM). HRTEM (High Resolution Transition Electron Microscope) images were registered with a JEOL 3010-UHR with acceleration potential of 300 kV. For these measurements, samples were dispersed on a copper grid covered with a lacey carbon film.

Table 1
Composition, structural parameters and BET surface area of Ni-$CeZrO_2$ catalysts.

Sample	Chemical composition[a]	SSA[b] (m^2/g)	Crystallite size[c] (nm)	
			NiO	$CeZrO_2$
A	$Ni(14.60)–Ce_{0.88}Zr_{0.15}O_2$	134	5.0	6.4
B	$Ni(14.81)–Ce_{0.90}Zr_{0.12}O_2$	97	9.9	7.7

[a] Calculated from EDS microanalysis.
[b] Calculated with BET equation.
[c] Calculated from XRD data with Scherrer equation.

The resulting images (Figs. 2 and 3) unfortunately suffer from a technical problem, related to the detector electronics, resulting in different background darkness in two halves of the images.

In situ adsorption experiments were carried out with Fourier Transform Infrared spectroscopy (FTIR) using carbon monoxide (CO) as probe molecule on a Bruker IFS 88 spectrometer equipped with mercury cadmium telluride (MCT) detector (64 accumulated scans, resolution 4 cm^{-1}). Samples were in form of self supporting pellets (10–12 mg/cm^2) and were directly treated in a quartz IR cell equipped with KBr windows, allowing thermal treatments in vacuum or in controlled atmosphere and recording the spectra at room temperature (RT) and liquid nitrogen temperature (estimated temperature 110 K). Background subtracted reported spectra were obatined by employing the spectrum of the catalysts before CO adsorption as reference.

Prior to FTIR studies the catalysts were outgassed at 823 K and oxidised at the same temperature in 60 Torr O_2 for 1 h. The same procedure was carried out for reduction treatments, employing 60 Torr of H_2 at 823 K. O_2 and H_2 were outgassed at the treatment temperature before cooling to room temperature (RT) in vacuum. High purity O_2, H_2 and CO were supplied by PRAXAIR, Belgium. Gases were passed through a liquid nitrogen trap before adsorption, and they were used without further purification.

Catalytic tests were carried out in a tubular fixed-bed stainless steel reactor (inner diameter 8 mm, length 24 cm), with the catalysts sitting on a porous plate. Flow and composition of reactants (water and CH_4) were monitored with mass flow controllers. Both reactants were pre-heated at 433–473 K before mixture, to avoid water vapour condensation. Reactor was heated with a heating jacket (max $T = 1073$ K) and located in a hot box (max $T = 473$ K). Reaction products were flowed through a gas–liquid separator, to condense unreacted water. The resulting dry products mixture was sent to a silica gel column for further dehydration and analysed online employing Gas Chromatography and an Advance Optima analyser (ABB), allowing thermal conductivity, electrochemical and spectrophotometric measurements in parallel. The system is calibrated to measure H_2, CO_2, CO (ppm), CH_4 and O_2.

Before the tests the catalysts (200 mg) were pressed into pellets with sizes between 255 and 350 μm and reduced at 673 K in a nitrogen flow containing 5% H_2 for 1 h. MSR tests were carried out at $P = 1$ atm, $T = 793$ K and GHSV = 30,000 h^{-1}, with steam to carbon ratios (S/C) = 2 and 3. Catalysts stability was checked by running the reaction for 250 h. After the tests the catalysts were cooled to RT in N_2 flow.

3. Results and discussion

3.1. General properties

Table 1 summarises the main characteristics of the prepared and tested catalysts. Both samples show a chemical composition very similar to the theoretical values employed for the synthesis. The main differences between catalysts A and B are in the measured SSA and crystallite size estimated from XRD

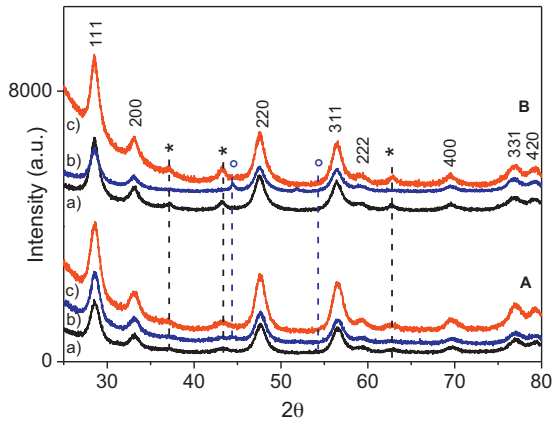

Fig. 1. XRD patterns of the Ni-$CeZrO_2$ catalysts, bottom (A) and top (B). The curves refer to catalysts: a) as prepared, b) reduced in H_2 at 673 K and c) after catalytic tests. Indexed peaks refer to the cubic $CeZrO_2$ phase, while peaks labelled with * and ◦ correspond to cubic NiO and Ni phases, respectively.

(see below). As for textural properties, it is noteworthy that the co-precipitation/digestion method allowed to obtain high SSA in both samples, irrespective of pH control. However, the best value (134 m^2/g) was obtained for catalyst A, prepared at pH 10.5. As for the samples porosity, which is the result of interparticle voids, it is not particularly affected by the pH control.

The XRD patterns of catalysts A and B as prepared (calcined), reduced in H_2 and after the catalytic tests are reported in Fig. 1. Both samples show the characteristic reflections corresponding to the cubic (fluorite) structure, labelled in the figure to the corresponding crystallographic planes (JCPDS 34-0394 for cubic CeO_2). The cell parameter a_0, calculated measuring the position of the (1 1 1) peak at around 28.58◦ is 5.40 Å, which is an intermediate value between that of pure CeO_2 and that of a cubic $Ce_{0.6}Zr_{0.4}O_2$ phase (JCPDS 38-1439), confirming the formation of a solid solution.

It is important to notice that, due to the broad character of the XRD peaks, the heterogeneity of ceria-zirconia mixed oxides structures cannot be excluded. In fact, different authors have shown how cubic and tetragonal phases are not easily distinguished on the basis of XRD, so that Raman spectroscopy was employed to this aim through the analysis of skeletal IR vibrations [31]. More recently, Montini et al. proposed the employ of Eu^{3+} as a structural probe, to monitor the presence of small metastable domains in $CeZrO_2$ samples with nanoscale heterogeneity, which appeared homogeneous by conventional XRD [32]. In our case, Raman measurements showed the presence of a single peak at 470 cm^{-1}, confirming that the main crystal phase is the cubic fluorite-like one (Fig. 1 in SI) [31]. We cannot however exclude a nanoscale heterogeneity, which could have important effects on the catalytic properties [32].

In addition to the $CeZrO_2$ peaks, in the as prepared samples weak peaks are observed at 37.09◦, 43.22◦ and 62.75◦, which can be related to the (1 1 1), (2 0 0) and (2 2 0) planes of a cubic NiO phase (JCPDS 47-1049, labelled with a star in Fig. 1). Noticeably, these peaks are weaker and broader in catalyst A, suggesting smaller size and higher dispersion of the NiO phase. Accordingly, the average crystallite sizes of both support and active phase were determined with the Scherrer equation from the line-widths of the peaks at $2\theta = 28.6°$ and 43.3◦, related to the (1 1 1) and (2 0 0) planes of $CeZrO_2$ and NiO phases, respectively. The calculated values (Table 1) clearly show an effect of the synthesis conditions on the dispersion of the active phase. While the average crystallite size of the support is similar in the two samples (around 6 nm), smaller NiO particles are formed when the synthesis pH is raised from 9.5 to 10.5.

The same XRD measurements were carried out on the catalysts previously reduced in H_2 and recovered after the catalytic tests (curves b and c, respectively). The reductive treatment is in fact necessary to form the Ni^0 active phase, responsible for the catalytic activity. To perform XRD (and HRTEM) experiments, samples were reduced in H_2 in cells connected to vacuum lines, and opened to atmosphere before the experiments. In sample B (top curve b), this treatment causes the disappearance of the peaks due to NiO, with formation of distinct features assigned to the cubic Ni^0 phase (JCPDS 4-0850, labelled with a circle in Fig. 1). The line-width of these peaks suggest a slight increase in the Ni^0 particle size (10 nm), which are stable in air.

Noticeably, the redox behaviour of supported Ni particles in sample A is different. When it is opened to atmosphere after the reductive treatment, the sample colour rapidly changes from black to dark brown, as the result of an exothermic reaction. The resulting XRD pattern is reported in Fig. 1 (bottom curve b). Notwithstanding their weakness and broadness, peaks related to NiO are still observable, suggesting a re-oxidation of Ni^0 particles upon air exposure. A very weak peak at $2\theta = 44.4°$ is also present, which could be due to a fraction of Ni^0 particles stable to atmosphere. This phenomenon will be rationalised in the following, when analysing the catalysts surface properties (Section 3.3). On the basis of XRD data the re-oxidation in air after reduction does not sensibly affect NiO particle size with respect to the calcined material.

As for the catalysts recovered from catalytic tests (curves c in Fig. 1), the results suggest negligible changes in the structure and average crystallite dimensions of both support and active phase, which is found in the form of NiO, as in the as-prepared materials. This implies an oxidation of the Ni^0 metal active phase during the catalytic reaction or the following steps (cooling in nitrogen and removal from reactor).

3.2. HRTEM measurements

HRTEM technique was employed to get additional information on the catalysts particle size and morphology. The measurements were carried out on the as-prepared, reduced and recovered catalysts, in analogy with XRD characterisation procedures. In this case the reduction treatment was also aimed at improving the contrast between the relatively "light" supported nickel phase and the "heavy" support [33]. For brevity, only the HRTEM images obtained on the reduced and recovered samples will be discussed in detail.

Fig. 2 reports some representative HRTEM images of sample A measured after reduction (a and b) and after the catalytic tests (c and d). The sample is characterised by well defined crystalline $CeZrO_2$ particles (5–6 nm average size, in very good agreement with XRD estimation), with spherical/hexagonal morphology. The shape of the particles indicates a degree of defective termination of the crystallites, as revealed by the roundish contours. The typical lattice distances of (1 1 1), (2 0 0) and (2 2 0) planes could be measured in most particles, having intermediate values between the references CeO_2 and $Ce_{0.6}Zr_{0.4}O_2$ phases (JCPDS 34-0394 and 38-1439, respectively).

Due to the low contrast between Ni and the support atoms, the analysis of Ni^0/NiO particles size and morphology was not straightforward and was carried out mainly by FT analysis, in order to highlight regions where characteristic lattice distance or Ni^0 or NiO crystal phases are dominant. Some of the monitored particles are outlined in Fig. 2 (dashed ellipsoids and rectangles). In the case of reduced catalyst A mainly NiO ellipsoid particles could be observed, with larger size and distinctly different morphology (circled region in Fig. 2b, measuring around 10 nm × 18 nm) with respect to the support. No statistical analysis

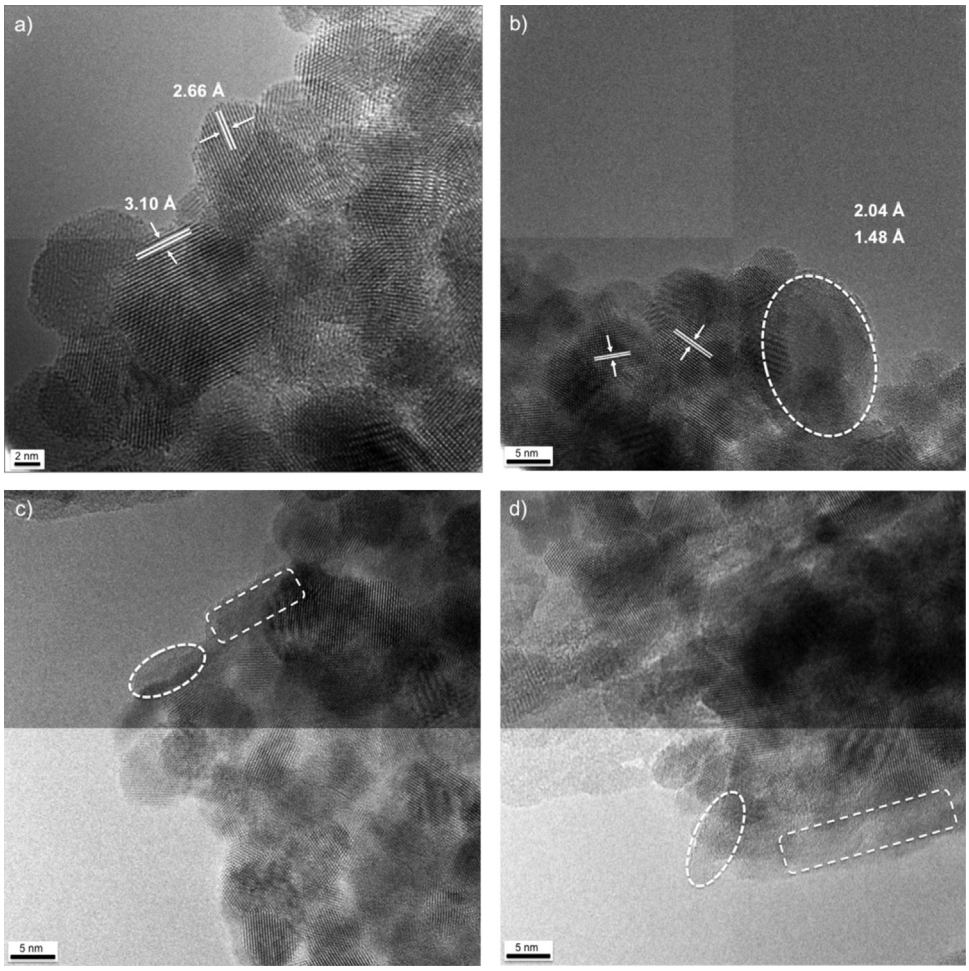

Fig. 2. HRTEM images of catalyst A. Sectors a and b: after reduction (magnification 600K× and 400K× respectively). Sectors c and d: after catalytic tests (magnification 400K×). For the meaning of dashed rectangles and ellipses see the text.

could be performed on these particles, since only few ones could be observed, with sizes and shapes similar that reported in Fig. 2b.

The size and morphology of the $CeZrO_2$ particles are unaffected by the catalytic tests. Small changes can be observed for the Ni active phase, still showing the ellipsoid particles (10 nm × 4 nm in both Fig. 2c and d) and larger ones with different elongated rectangular shape. Due to the low contrast between active phase and support, we cannot exclude the presence of very small, highly dispersed Ni/NiO particles, too small to be detected by HRTEM.

Size and morphology of the $CeZrO_2$ support of sample B (Fig. 3a) are similar to A. However, in this case larger Ni particles could be observed after reduction, as the one (35 nm × 22 nm) highlighted in Fig. 3b. The measured lattice distance (2.03 Å) suggests that we are observing the cubic Ni^0 phase, in agreement with XRD. As observed in the case of catalyst A, the support morphology is unchanged after the catalytic tests, but large NiO aggregates with irregular morphology are formed, as the one shown in Fig. 3c (32 nm × 40 nm). Moreover, large amorphous portions of matter are observed (Fig. 3d, 22 nm × 50 nm), embedding the support particles, which are probably due to carbon residues from the methane steam reforming process. Interestingly, these carbon deposits do not show any graphene structure or filament shape, in contrast to what often observed on Ni-based catalysts [7,12]. This difference could be related to the different conditions employed in the catalytic tests.

3.3. Surface studies

The surface properties of the catalysts were investigated by FTIR spectroscopy, particularly employing the CO molecular probe. In this work, the attention is focused on the CO stretching region (νCO), while the spectra measured in the OH stretching region (νOH) are not reported for sake of brevity. We only mention that this region is quite complicated, as often observed in ZrO_2 or $CeZrO_2$ oxides [34–36]. A discussion of these features is outside the scope of this paper, however we have to acknowledge the presence of a narrow band at 3740 cm^{-1}, which could be ascribed to surface Si–OH groups [36], formed as a result of Si contamination from glassware during the high pH synthesis. This aspect should be considered when reproducing the synthesis, since it has been shown that Si can improve the redox ability of $CeZrO_2$ catalysts [37].

The CO adsorption experiments were carried out in two steps: i) gradual increase of CO equilibrium pressure (P_{CO}) at 110 K; ii) increase of temperature from 110 K to RT at P_{CO} = 20 Torr [33]. For simplicity, a selection of the more informative experiments is reported and discussed in the following. The spectra are quite complex, and they can be divided into three regions: i) from 2250 to 2100 cm^{-1}, ii) from 2100 to 2000 cm^{-1}, iii) 2000 to 1800 cm^{-1} [33,38–41].

3.3.1. Evolution of CO spectra with coverage at 110 K

First, the Infrared spectra measured at 110 K while increasing P_{CO} on catalyst A previously oxidised or reduced (Fig. 4 top and

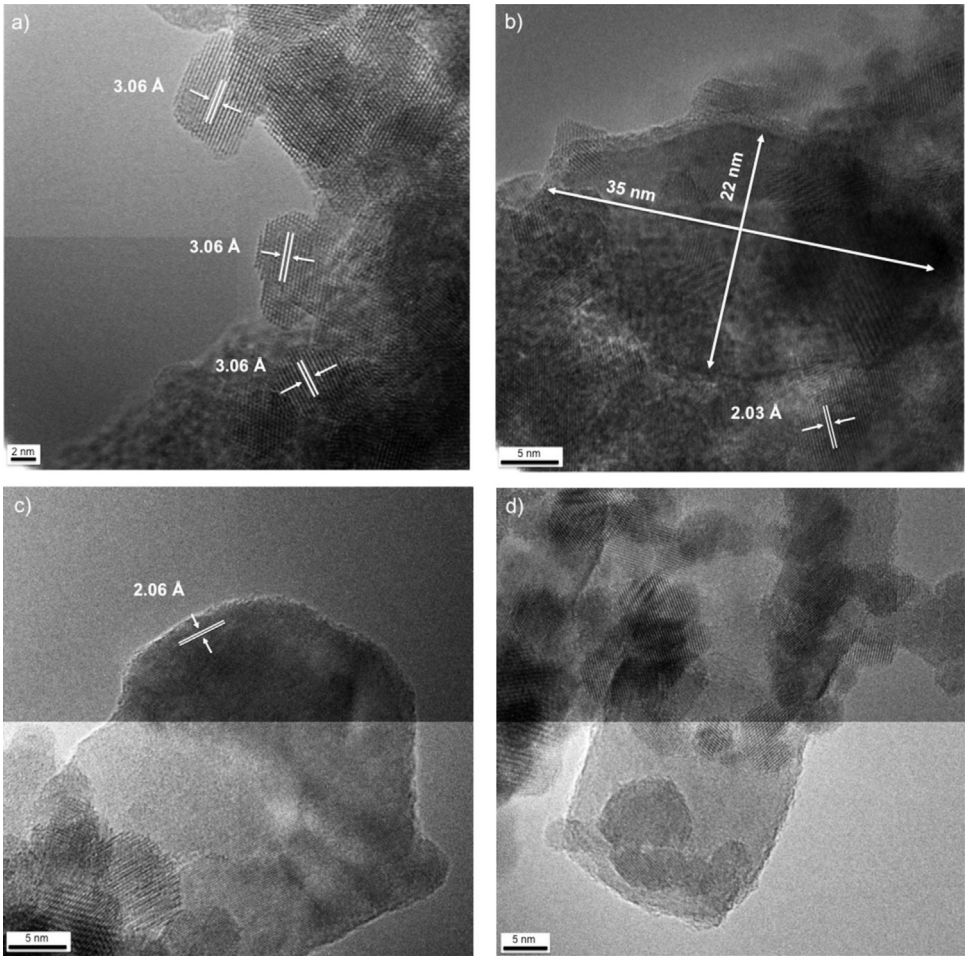

Fig. 3. HRTEM images of catalyst B. Sectors a and b: after reduction (magnification 600K× and 500K× respectively). Sectors c and d: after catalytic tests (magnification 500K× and 400K× respectively).

bottom respectively), will be discussed. The results obtained in the same conditions on sample B, being similar, are not reported for brevity. The spectra obtained on the oxidised sample (Fig. 4, top panel) are mainly found in the 2250 – 2100 cm^{-1} region, even if minor features are also present at lower frequency. At intermediate P_{CO} four components at 2177, 2162, 2146 and 2100 cm^{-1} can be appreciated, with one at 2172 cm^{-1} dominating at low coverage (dashed–dotted curve). Their relative intensity and position change with coverage, so that at high P_{CO} (short-dashed line) the spectra are dominated by a narrow peak at 2158 cm^{-1}, with shoulders at 2172 and 2138 cm^{-1}. The very weak absorption at 2100 cm^{-1} is only slightly affected by the coverage. When the same experiment is performed on the reduced catalyst (bottom panel) changes are observed in the whole spectral range. At high frequency, the component at 2172 cm^{-1} has disappeared, the one at 2158 cm^{-1} is less intense and shifted to 2162 cm^{-1}, while a third component grows at 2151 cm^{-1}. New weak bands are found at 2096, 2005, 1950 and 1905 cm^{-1}, all slightly affected by changes in CO coverage.

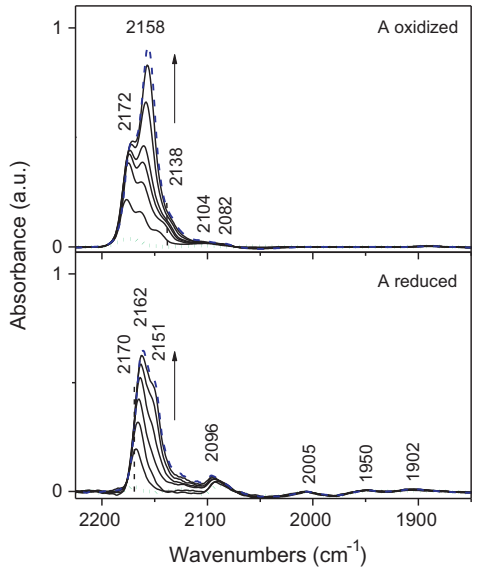

Fig. 4. FTIR spectra of increasing CO coverage from P_{CO} = 0.5 (short dotted) to 20 Torr (dashed) at 110 K on catalyst A oxidised (top) and reduced (bottom panel).

First, the attention will be focused on the high energy bands, which are dominated by the contribution of the support surface sites. More in detail, the band at 2158/2162 cm^{-1} can be safely assigned to the formation of CO adducts with Ce^{4+} sites on relatively extended surfaces, while the component at 2138/2151 cm^{-1}, growing after the reduction treatment is compatible with Ce^{3+} sites [39–42]. The band at 2172 cm^{-1}, shifting with coverage on the oxidised sample and disappearing after reduction is more controversial, since bands in similar positions were found for CO adducts on defective (coordinatively unsaturated) Ce^{4+} [41,42], Zr^{4+} [34], or Ni^{2+} ions [43–46]. On the basis of the comparison with CO spectra measured on $CeZrO_2$ support prepared by similar conditions (Fig. 2 in SI), the most likely interpretation of this band is in terms of Ni^{2+} ions on the surface of the NiO particles detected by HRTEM, even if

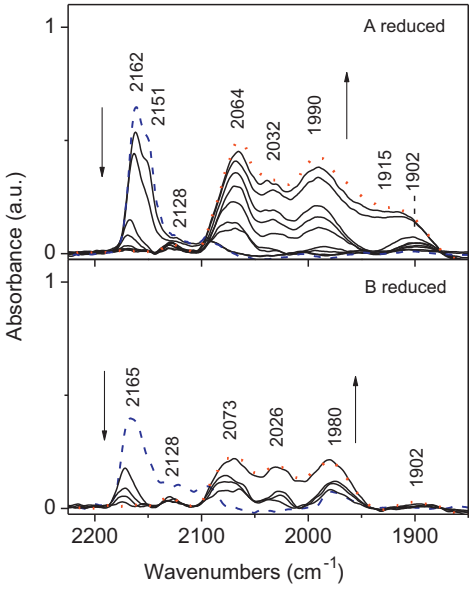

Fig. 5. Evolution of CO FTIR spectra (P_{CO} = 20 Torr) from 110 K (dashed) to RT (dotted) on reduced catalysts A and B (top and bottom, respectively).

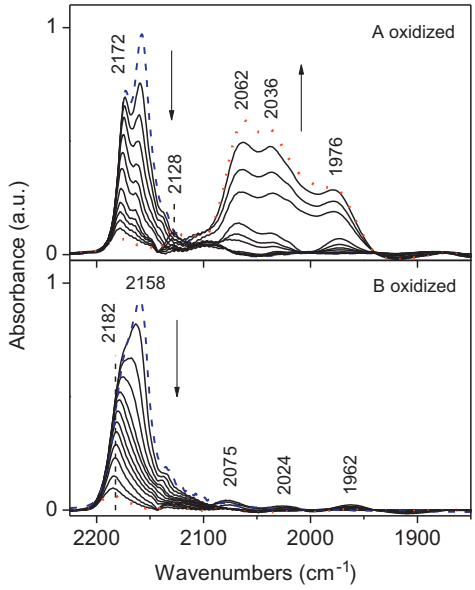

Fig. 6. Evolution of CO spectra (P_{CO} = 20 Torr) from 110 K (dashed) to RT (dotted) on oxidised catalysts A and B (top and bottom, respectively).

we cannot exclude a minor contribution from Zr^{4+} and uncoordinatively unsaturated Ce^{4+}. This interpretation is in agreement with the observed shift with coverage, which would not be compatible with Ce^{4+} ions present on steps or edges or with isolated Zr^{4+} ions in a ceria matrix. The presence of Ni^{+} ions, which are expected to form CO adducts between 2145 and 2100 cm^{-1} is not evident.

As for the low frequency bands, the one at 2096 cm^{-1} evident on the reduced sample can be safely assigned to linear carbonyl formed on the surface of Ni^0 particles, while the bands between 2000 and 1800 cm^{-1} (2005, 1950 and 1905 cm^{-1}) are typical of Ni^0 bridged CO complexes [33,38].

3.3.2. Evolution of CO spectra from 110 K to RT

The second part of the CO adsorption experiments is reported for both catalysts, in order to highlight their different behaviour. Fig. 5 reports the spectra obtained by increasing temperature from 110 K to RT at high CO coverage on the reduced catalysts (A and B, top and bottom respectively). For both samples the high frequency region (2250–2100 cm^{-1}) shows the gradual decrease of the bands assigned to CO adducts on Ce^{4+} and Ce^{3+} ions, in agreement with the weak character of the related CO adducts, and with what observed on bare $CeZrO_2$ support upon outgassing adsorbed CO at 110 K (Fig. 2 in SI). On the contrary the temperature increase causes the gradual growth of broad bands between 2100 and 1800 cm^{-1}, more intense on catalyst A, and of a component at 2128 cm^{-1}.

Bands in the 2100–1800 cm^{-1} region have been often observed while sending CO on supported Ni^0 particles, and their nature, evolution upon pressure, temperature and evacuation were deeply investigated in many papers [33,38]. In this work, their discussion will be based on the recent conclusions drawn by Morandi et al. [33], where interested readers can find more details. Shortly, bands similar to those observed at 2064, 2032 and 1990 cm^{-1} on catalyst A (2073, 2026 and 1980 cm^{-1} on catalyst B) were assigned to volatile mono-nuclear $Ni(CO)_y$ ($y \leq 4$), formed by reaction between CO and high energy Ni^0 surface sites, and then adsorbed on the support. Less clear is the assignment of the components at 1915 and 1902 cm^{-1}, that could be related to polynuclear $Ni_x(CO)_y$ formed by similar mechanism [33]. More in detail, on the basis of their evolution upon evacuation and subsequent CO dosage, Morandi et al. assigned components at 2010, 1930 and 1875 cm^{-1} to polynuclear $Ni_x(CO)_y$ species formed upon agglomeration of mononuclear ones during the outgassing at RT, while bands at 2020, 1973 and 1915 cm^{-1} were related to $Ni_x(CO)_y$ species with higher CO/Ni ratio [33]. Without entering in the details of this complex reactivity, which has been deeply studied in the literature, the presence of these bands is a clear signal of the fact that reactive Ni^0 atoms are present on the surface of small particles.

In agreement with previous reports [33,38], these experiments confirm the high reactivity of surface Ni^0 atoms, which are easily extracted by interaction with CO to form volatile complexes. This could be explained either with the presence of highly dispersed Ni particles, too small to be detected by HRTEM, or by defective high index surfaces [7,33]. Noticeably, this reactivity is higher on catalyst A, showing the more intense $Ni(CO)_y$ and $Ni_x(CO)_y$ bands.

As for the band at 2128 cm^{-1}, its position resemble that of the forbidden $^2F_{5/2} \rightarrow {}^2F_{7/2}$ electronic transition of Ce^{3+} ions [39], but the narrow character and the observed evolution with CO reactivity do not favour this assignment. We thus assign it to $Ni^{+}(CO)$ adducts, formed on partially reduced sites.

When the same experiments are carried out on the oxidised samples, the spectra reported in Fig. 6 are observed. Similarly to what described above, temperature increase causes the gradual depletion of the high energy bands, related to weak CO adducts on Ce^{4+} and Ni^{2+} ions. Interestingly, on catalyst A this is accompanied by the growth of the broad bands 2062, 2036 and 1976 cm^{-1} and of the component at 2128 cm^{-1}, similarly to what observed after reduction. This implies that in this sample Ni^0 particles are formed upon CO adsorption even after an oxidation pre-treatment. Clearly, this can be ascribed to a reduction process caused by CO, which is favoured on the catalyst with smaller or more defective NiO particles. Notice that the reduction process results also in the formation of Ni^{+} ions, particularly in catalyst A, so that we can ascribed this band to Ni^{+} ions on the surface of small, partially reduced NiO particles. Next paragraph is devoted to rationalise these phenomenon by drawing simplified surface models.

3.4. Rationalisation of surface reactivity of catalyst A

The characterisation data described above points to the occurring of two distinct redox processes, taking place on the catalyst

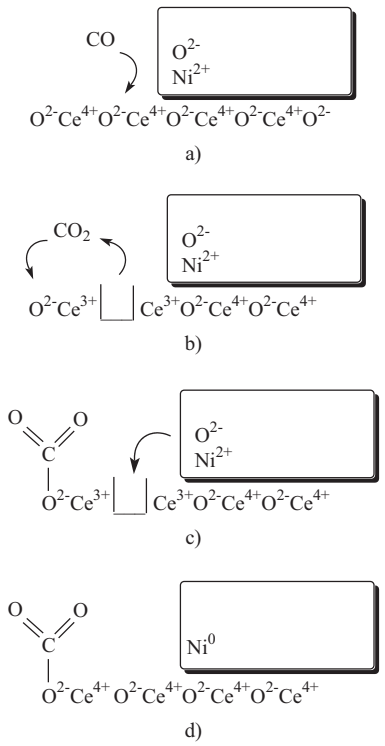

Scheme 1. Simplified representation of room temperature Ni-$CeZrO_2$ surface reduction upon CO interaction, forming adsorbed carbonates species and Ni^0 particles.

with smaller and better dispersed Ni particles (sample A). Namely, this includes: i) reduction of NiO particles to Ni^0 upon CO contact (temperature increasing from 110 K to RT) and ii) RT oxidation of Ni^0 to NiO upon air exposure. Both phenomena have been rationalised by considering NiO/Ni^0 particles in intimate contact with $CeZrO_2$ support, where for simplicity only surface Ce ions are depicted (Schemes 1 and 2). This choice is related to the fact that structural and spectroscopic techniques mainly show features ascribable to CeO_2 oxide, likely because of the relatively low Zr contents. This does not mean that these ions do not play a role, since it has been reported that their inclusion in the ceria lattice, besides improving thermal stability, confer better redox and OSC properties [26].

Scheme 1 describes the effect of CO adsorption on the oxidised catalyst (panel a). This is an oversimplified scheme since it does not includes CO adsorption on Ce^{4+}/Ce^{3+} ions and NiO/Ni^0 particles. Due to the basicity of the ceria support, CO can react with the surface to form CO_2, which in turns adsorbs on other basic surface oxygen atoms to form stable carbonates (Scheme 1b and c). This process is well known and results in the formation of complex carbonates bands in between 1700 and 1000 cm^{-1} [42,47] (Fig. 3 in SI). This process results in the formation of oxygen vacancies on ceria surface, which can be re-established by oxygen removal from supported NiO (Schemes 1c and d). The resulting stoichiometric reactions are the following:

$$2Ce^{4+} + O^{2-} + CO \rightarrow 2Ce^{3+} + CO_2 \quad (1)$$

$$2Ce^{3+} + Ni^{2+} \rightarrow 2Ce^{4+} + Ni^0 \quad (2)$$

In this context, we recall the fact the a different reactivity path was proposed for CO oxidation on NiO particles supported on ZrO_2 at 773 K, without requesting the involvement of the support [48]. Even if the mechanism proposed in Ref. [48] is reasonable, in our case CO oxidation is observed at low temperature, and this can be easily explained by considering the important oxygen storage capability (OSC) of the ceria-based support. In the reported scheme the role of surface Zr ions has not been considered as playing an active role, mainly because of the relatively low concentration. However, previous reports have clearly shown that the insertion of Zr ions into the ceria lattice has a positive effect on its OSC, improving redox properties and lowering the reduction temperature [26]. Finally, we have to acknowledge the possible contamination of the oxide surface with traces of Si, which has also been reported to improve $CeZrO_2$ redox properties [37].

The surface model employed to explain the reduction of NiO to Ni^0 by RT CO interaction can be also employed to rationalise the opposite redox behaviour, that is the re-oxidation of Ni^0 upon air exposure (see above, Section 3.1). This was carried out by drawing Scheme 2, showing as a starting point a reduced catalyst surface, characterised by Ni^0 particles in contact with a partially reduced ceria surface (panel a), showing Ce^{3+} ions and oxygen vacancies. When contacted with molecular oxygen, reduced ceria surface quickly reacts, dissociating the O_2 molecule to fill one vacancy (Scheme 2b). It could be thus proposed that this process generates highly reactive oxygen species that could be easily transferred to Ni^0 particle in close contact with the support to form NiO (Scheme 2c). At this stage it is not possible to draw a more detailed mechanism for O_2 dissociation with respect to what depicted in panel 2b. However, we cannot exclude the formation of intermediate oxygen species (superoxides, etc.).

The resulting stoichiometric reactions are the following:

$$2Ce^{3+} + \tfrac{1}{2}O_2 \rightarrow 2Ce^{4+} + O^{2-} \quad (3)$$

$$Ni^0 + \tfrac{1}{2}O_2 \rightarrow NiO \quad (4)$$

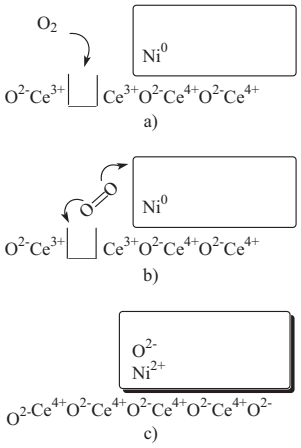

Scheme 2. Simplified representation of room temperature oxidation of a previously reduced Ni-$CeZrO_2$ surface as a result of contact with atmosphere.

3.5. Catalytic tests

Methane steam reforming reaction was performed on the two catalysts to evaluate their activity at a relatively low temperature (793 K) and to test their stability in the reaction conditions. S/C ratio was varied from 2 to 3 by keeping constant temperature and spatial velocity. For brevity only the results obtained at S/C = 2 are reported in Fig. 7, showing the dry gas composition as a function of time on stream. The values measured at both S/C ratios after 24 and 250 h reaction are summarised in Table 2 for both catalysts.

When the steam to carbon ratio is 3, catalyst A show a hydrogen production close to the thermodynamic value in the same temperature and pressure conditions, with only a slight conversion decrease with time on stream (Table 2). This decrease could be related to small temperature variations along the reaction: since the flow is very low, methane conversion is affected by even tiny

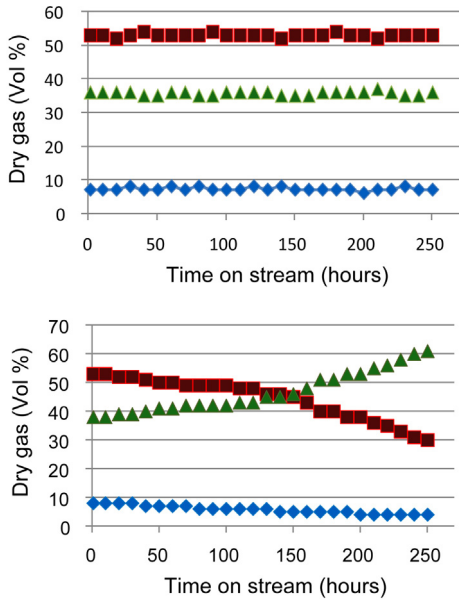

Fig. 7. Dry gas composition (squares = H_2; triangles = CH_4; diamonds = CO_2) as a function of time on stream for MSR carried out at 793 K, GHSV = 30,000 h^{-1}, S/C = 2 and P = 1 atm on catalysts A (top) and B (bottom).

temperature oscillations. The CO production is almost negligible. This implies that water gas shift reaction (WGS), the exothermic reaction involving CO molecules produced from methane reforming, takes place together with MSR. This is in agreement with literature, since it has been reported that the acid/base properties of the $CeZrO_2$ support have a positive effect on WGS [49].

When the reaction is carried out at S/C = 2, hydrogen conversion is lower, but its value remains practically constant during the whole 250 h reaction (Fig. 7, top panel). Also in this case CO production is negligible, indicating that WGS reaction is efficient even at low water content. Notice that these conditions are favourable from an energetic point of view, since less energy is required to vapourise water in the reactants feed, but are particularly harsh for catalysts stability, due to the high carbon content in the feed.

The catalytic activity of catalyst B is similar during the first hours of reaction at both S/C ratios (Table 2). However, in this case deactivation with time on stream is evident after 150 h, particularly at S/C = 2 (Fig. 7 bottom panel and Table 2). This is not surprising since one of the main reasons for deactivation is related to the deposition of carbon on the catalyst surface, phenomenon that is favoured at low S/C ratios. Noticeably, large amorphous particles were indeed observed by HRTEM on recovered catalyst B (see above).

Table 2
Dry mixture composition (vol%) of syngas obtained on Ni-$CeZrO_2$ catalysts at 793 K, GHSV = 30,000 h^{-1} and P = 1 atm.

	Time on stream (h)	CH_4	H_2 (vol%)	CO_2
A				
S/C = 3	24	25.7	66.8	10.4
	250	26.6	64.1	10.3
S/C = 2	24	38.1	52.9	8.5
	250	37.2	54.5	8.7
B				
S/C = 3	24	29.5	61.2	8.7
	250	34.6	57.2	7.6
S/C = 2	24	39.6	52.4	8.4
	250	61.7	30.2	4.4

On the whole, these results show only a minor effect of Ni dispersion on the catalytic activity in low temperature MSR, since the initial conversion values of the two catalysts are similar. However, catalyst deactivation is observed on the sample with bigger Ni particles, as a consequence of carbon deposition, particularly at low S/C ratios. On the contrary, the good stability of catalysts A can be related to the high dispersion of Ni particles on the $CeZrO_2$ support, allowing oxygen availability which is unfavourable to carbon deposition.

4. Conclusions

Two different $NiCeZrO_2$ catalysts, with similar chemical composition were synthesised by one pot co-precipitation, and fully characterised. XRD and HRTEM analysis showed similar size and morphology of the $CeZrO_2$ support, being characterised by small (5–6 nm) roundish particles. On the contrary, the particle size of supported NiO/Ni^0 particles was strongly affected by the synthesis conditions, particularly pH. Moreover, catalyst A, the sample with smaller NiO particles, showed a peculiar surface reactivity, testified by the fast oxidation of previously reduced Ni^0 particles when exposed to air.

FTIR spectroscopy was employed to monitor the catalysts surface properties, by employing CO adsorption experiments as a function of pressure or measurement temperature. These results showed the formation of volatile mono and poly-nuclear carbonyls on both reduced catalysts, indicating the presence of highly reactive Ni^0 ions, in very small particles (below the detection limit of HRTEM) or on defective surfaces of large ones. Moreover, similar carbonyls were formed on the catalyst with the highest Ni dispersion even without a reducing pretreatment. These evidences allowed us to propose surface reaction mechanisms, involving NiO/Ni^0 particles in intimate contact with the $CeZrO_2$ surface, allowing easy oxygen transfer. On the basis of the reported results it is not possible to infer if these effects take place between the support and the Ni particles (5–10 nm) observed by HRTEM, or if they are related to smaller particles, below the detection limits of HRTEM, as recently proposed for a series of Au/$CeZrO_2$ catalysts [49].

Both catalysts show a good activity in MSR reaction at 793 K. At S/C = 3 H_2 production is in fact close to the thermodynamic upper limit. The negligible formation of CO indicates that WGS reaction is taking place together with MSR, and this reactivity can be ascribed to the acid/base properties of the $CeZrO_2$ support, activating adsorbed water molecules. Noticeably, the different morphological and surface properties of the two catalysts, as evidenced by characterisation, justify a different stability with time on stream: while catalysts A is stable at both S/C ratios, catalyst B deactivates at harsher conditions (S/C = 2), with formation of carbon patches, as testified by HRTEM. This indicates an important effect of the $CeZrO_2$ support on Ni catalytic activity, which could be explained with an enhanced oxygen transport from ceria to Ni particles in intimate contact with its surface. Even if the models employed to explain the surface reactivity are based on a simplified ceria surface, the observed low temperature activity towards CO or air can be ascribed to the positive effect of Zr ions insertion into the ceria lattice, which has been shown to increase OSC an redox properties [26].

Acknowledgements

Italian Ministry of the Environment and of the Territory and Sea Protection (MATT) is gratefully acknowledged for funding project METISOL. We thanks S. Morandi and G. Ghiotti for fruitful discussion, G. Gatti, from Dipartimento di Scienze ed Innovazione

Tecnologica of Università del Piemonte Orientale for Raman measurements.

Appendix A. Supplementary data

Supplementary data associated with this article can be found, in the online version, at http://dx.doi.org/10.1016/j.apcatb.2013.02.036.

References

[1] M. De Falco, A. Giaconia, L. Marrelli, P. Tarquini, R. Grena, G. Caputo, International Journal of Hydrogen Energy 34 (2009) 98–109.
[2] A. Giaconia, M. de Falco, G. Caputo, R. Grena, P. Tarquini, AIChE Journal 54 (2008) 1932–1944.
[3] J.R. Rostrup-Nielsen, J. Sehested, J.K. Norskov, Advances in Catalysis 47 (2002) 65–139.
[4] X. Wang, R.J. Gorte, Applied Catalysis A: General 224 (2002) 209–218.
[5] A.M. Gadalla, M.E. Sommer, Chemical Engineering Science 44 (1989) 2825–2829.
[6] Y. Matsumura, T. Nakamori, Applied Catalysis A: General 258 (2004) 107–114.
[7] A. Parmaliana, F. Arena, F. Frusteri, S. Coluccia, L. Marchese, G. Martra, A.L. Chuvilin, Journal of Catalysis 141 (1993) 34–47.
[8] J.A. Lercher, J.H. Bitter, W. Hally, W. Niessen, K. Seshan, Studies in Surface Science and Catalysis 101 (1996) 463–472.
[9] L. Zhou, Y. Guo, Q. Zhang, M. Yagi, H. Li, J. Chen, M. Sakurai, H. Kameyama, Catalysis Communications 10 (2008) 325–329.
[10] J. Xu, L. Chen, K.F. Tan, A. Borgna, M. Saeys, Journal of Catalysis 261 (2009) 158–165.
[11] H.S. Bengaard, J.K. Norskov, J. Sehested, B.S. Clausen, L.P. Nielsen, A.M. Molenbroek, J.R. Rostrup-Nielsen, Journal of Catalysis 209 (2002) 365–384.
[12] J.H. Larsen, I. Chorkendorff, Surface Science Reports 35 (1999) 165–222.
[13] H.S. Roh, H.S. Potdar, K.W. Jun, J.W. Kim, Y.S. Oh, Applied Catalysis A: General 276 (2004) 231–239.
[14] S. Xu, X. Yan, X. Wang, Fuel 85 (2006) 2243–2247.
[15] K. Wang, X. Li, S. Ji, X. Shi, J. Tang, Energy and Fuels 23 (2009) 25–31.
[16] P. Kumar, Y. Sun, R.O. Idem, Energy and Fuels 21 (2007) 3113–3123.
[17] A. Martinez-Arias, J.M. Coronado, R. Cataluna, J.C. Conesa, J. Soria, Journal of Physical Chemistry B 102 (1998) 4357–4365.
[18] P. Bera, S. Mitra, S. Sampath, M.S. Hegde, Catalysis Communications (2001) 927–928.
[19] D.K. Kim, K. Stoewe, F. Mueller, W.F. Maier, Journal of Catalysis 247 (2007) 101–111.
[20] A. Caballero, J.P. Holgado, V.M. Gonzalez-delaCruz, S.E. Habas, T. Herranz, M. Salmeron, Catalysis Communications 46 (2010) 1097–1099.
[21] A. Trovarelli, Chemical Reviews 38 (1996) 439–520.
[22] C.T. Campbell, C.H.F. Peden, Science 309 (2005) 713–714.
[23] F. Esch, S. Fabris, L. Zhou, T. Montini, C. Africh, P. Fornasiero, G. Comelli, R. Rosei, Science 309 (2005) 752–755.
[24] A. Trovarelli, F. Zamar, J. Llorca, C. deLeitenburg, G. Dolcetti, J.T. Kiss, Journal of Catalysis 169 (1997) 490–502.
[25] J. Kaspar, P. Fornasiero, M. Graziani, Catalysis Today 50 (1999) 285–298.
[26] M. Daturi, E. Finocchio, C. Binet, J.C. Lavalley, F. Fally, V. Perrichon, H. Vidal, N. Hickey, J. Kaspar, Journal of Physical Chemistry B 104 (2000) 9186–9194.
[27] M. Thammachart, V. Meeyoo, T. Risksomboon, S. Osuwan, Catalysis Today 68 (2001) 53–61.
[28] S. Damyanova, B. Pawelec, K. Arishtirova, M.V.M. Huerta, J.L.G. Fierro, Applied Catalysis A: General 337 (2008) 86–96.
[29] G. Colon, M. Pijolat, F. Valdivieso, H. Vidal, J. Kaspar, E. Finocchio, M. Daturi, C. Binet, J.C. Lavalley, R.T. Baker, S. Bernal, Journal of the Chemical Society, Faraday Transactions 94 (1998) 3717–3726.
[30] G. Balducci, M.S. Islam, J. Kaspar, P. Fornasiero, M. Graziani, Chemistry of Materials 12 (2000) 677–681.
[31] V.S. Escribano, E.F. Lopez, M. Panizza, C. Resini, J.M.G. Amores, G. Busca, Solid State Sciences 5 (2003) 1369–1376.
[32] T. Montini, A. Speghini, L. De Rogatis, B. Lorenzut, M. Bettinelli, M. Graziani, P. Fornasiero, Journal of the American Chemical Society 131 (2009) 13155–13160.
[33] S. Morandi, M. Manzoli, F. Prinetto, G. Ghiotti, C. Gerardin, D. Kostadinova, D. Tichit, Microporous and Mesoporous Materials 147 (2012) 178–187.
[34] C. Morterra, G. Cerrato, S. Di Ciero, Applied Surface Science 126 (1998) 107–128.
[35] M. Daturi, E. Finocchio, C. Binet, J.C. Lavalley, F. Fally, V. Perrichon, Journal of Physical Chemistry B 103 (1999) 4884–4891.
[36] F.C. Gennari, T. Montini, N. Hickey, P. Fornasiero, M. Graziani, Applied Surface Science 252 (2006) 8456–8465.
[37] E. Rocchini, A. Trovarelli, J. Llorca, G.W. Graham, W.H. Weber, M. Maciejewski, A. Baiker, Journal of Catalysis 194 (2000) 461–478.
[38] G. Martra, F. Arena, M. Baricco, S. Coluccia, L. Marchese, A. Parmaliana, Catalysis Today 17 (1993) 449–458.
[39] T. Tabakova, M. Manzoli, F. Vindigni, V. Idakiev, F. Boccuzzi, Journal of Physical Chemistry A 114 (2010) 3909–3915.
[40] M. Manzoli, R. Di Monte, F. Boccuzzi, S. Coluccia, J. Kaspar, Applied Catalysis B: Environmental 61 (2005) 192–205.
[41] M. Manzoli, F. Boccuzzi, A. Chiorino, F. Vindigni, W. Deng, M. Flytzani-Stephanopoulos, Journal of Catalysis 245 (2007) 308–315.
[42] C. Binet, M. Daturi, J.C. Lavalley, Catalysis Today 50 (1999) 207–225.
[43] K. Hadjiivanov, H. Knozinger, M. Mihaylov, Journal of Physical Chemistry B 106 (2002) 2618–2624.
[44] K. Hadjiivanov, M. Mihaylov, N. Abadjieva, D. Klissurski, Journal of the Chemical Society, Faraday Transactions 94 (1998) 3711–3716.
[45] K. Hadjiivanov, M. Mihaylov, D. Klissurski, P. Stefanov, N. Abadjieva, E. Vassileva, L. Mintchev, Journal of Catalysis 185 (1999) 314–323.
[46] D. Costa, G. Martra, M. Che, L. Manceron, M. Kermarec, Journal of the American Chemical Society 124 (2002) 7210–7217.
[47] C. Morterra, G. Magnacca, Catalysis Today 27 (1996) 497–532.
[48] V.M. Gonzalez-Delacruz, R. Pereniguez, F. Temero, J.P. Holgado, A. Caballero, ACS Catalysis 1 (2011) 82–88.
[49] F. Vindigni, M. Manzoli, T. Tabakova, V. Idakiev, F. Boccuzzi, A. Chiorino, Applied Catalysis B: Environmental 125 (2012) 507–515.